MR. BADR KHBOUZ (Orcid ID : 0000-0002-1253-0864)
DR PASCAL ROWART (Orcid ID : 0000-0002-4210-2713)

Article type : Regular Paper

The genetic deletion of the Dual Specificity Phosphatase 3 (DUSP3) attenuates kidney damage and inflammation following ischemia/reperfusion injury in mouse

B. Khbouz [1, *], P. Rowart [1, 2 *], L. Poma [1], E. Dahlke [4], M. Bottner [4], M. Stokes [5], G. Bolen [6], S. Rahmouni[7], F. Theilig [3, 4], F. Jouret [1,8]

1. *Groupe Interdisciplinaire de Génoprotéomique Appliquée* (GIGA), Cardiovascular Sciences, University of Liège (ULiège), Belgium
2. Department of Pharmacology and Chemical Biology, School of Medicine, University of Pittsburgh, United States.
3. Institute of Anatomy, Department of Medicine, University of Fribourg, Fribourg, Switzerland
4. Institute of Anatomy, Christian Albrechts-University, Kiel, Germany
5. Cell Signaling Technology, INC. Danvers, MA, USA
6. Department of Clinical Sciences, Fundamental and Applied Research for Animals & Health (FARAH), Veterinary Faculty, University of Liège (ULiège), Belgium
7. *Groupe Interdisciplinaire de Génoprotéomique Appliquée* (GIGA), Medical Genomics, University of Liège (ULiège), Belgium
8. Division of Nephrology, CHU of Liège, University of Liège (CHU ULiège), Belgium

Corresponding Author:

François Jouret, MD, PhD
University of Liège Academic Hospital, Division of Nephrology
Avenue Hippocrate, 13 – B4000 Liège, Belgium
E-mail: francois.jouret@chuliege.be

This article has been accepted for publication and undergone full peer review but has not been through the copyediting, typesetting, pagination and proofreading process, which may lead to differences between this version and the Version of Record. Please cite this article as doi: 10.1111/APHA.13735

Phone: +3243662540
Fax: +3243667205

Running Title: DUSP3 in renal ischemia/reperfusion

Abstract

Aim:
Dual Specificity Phosphatase 3 (DUSP3) regulates the innate immune response, with a putative role in angiogenesis. Modulating inflammation and perfusion contributes to renal conditioning against ischemia/reperfusion (I/R). We postulate that the functional loss of DUSP3 is associated with kidney resistance to I/R.

Methods:
Ten C57BL/6 male *WT* and *Dusp3*$^{-/-}$ mice underwent right nephrectomy and left renal I/R (30min/48h). Renal injury was assessed based on serum levels of urea (BUN) and Jablonski score. The expression of CD31 and VEGF vascular markers was quantified by RT-qPCR and immuno-staining. Renal resistivity index (RRI) was measured *in vivo* by Doppler ultrasound. Comparative phosphoproteomics was conducted using IMAC enrichment of phosphopeptides. Inflammatory markers were quantified at both mRNA and protein levels in ischemic vs. non-ischemic kidneys in *WT* versus *Dusp3*$^{-/-}$.

Results:
At baseline, we located DUSP3 in renal glomeruli and endothelial cells. CD31-positive vascular network was significantly larger in *Dusp3*$^{-/-}$ kidneys compared to *WT*, with a lower RRI in *Dusp3*$^{-/-}$ mice. Following I/R, BUN and Jablonski score were significantly lower in *Dusp3*$^{-/-}$ vs. *WT* mice. Phosphoproteomics highlighted a down-regulation of inflammatory pathways and up-regulation of phospho-sites involved in cell metabolism and VEGF-related angiogenesis in *Dusp3*$^{-/-}$ vs. *WT* ischemic kidneys. *Dusp3*$^{-/-}$ ischemic kidneys showed decreased mRNA levels of *CD11b*, *TNF-α*,

KIM-1, *IL-6*, *IL-1β* and *caspase-3* compared to controls. The numbers of PCNA-, F4-80- and CD11b-positive cells were reduced in *Dusp3*$^{-/-}$ vs. *WT* kidneys *post* I/R.

Conclusion:

Genetic inactivation of *Dusp3* is associated with kidney conditioning against I/R, possibly due to attenuated inflammation and improved perfusion.

Key words: acute kidney injury; DUSP3; kidney; phosphoproteomics; renal ischemia/reperfusion; sterile inflammation.

Introduction

Renal ischemia/reperfusion (I/R) injury is the leading cause of acute kidney injury (AKI) (1) and corresponds to the transient interruption of the renal blood flow leading to vascular and tubular dysfunctions (2-4). Typically, kidney transplantation and cardiothoracic surgery are clinical paradigms of renal I/R (5). Renal I/R induces a "sterile" inflammation (6), with a recruitment of mononuclear leukocytes and the production of pro-inflammatory cytokines and chemokines (7). The innate immune system contributes to renal I/R injury (8). One may thus hypothesize that modulating the innate immune response may attenuate the I/R-induced damage and preserve kidney architecture and function. Similarly, maintaining and/or expanding renal vascular density may help accelerate the perfusion and oxygenation of the organ following an ischemic insult (9, 10). These maneuvers form the core of renal ischemic conditioning (RIC) (11, 12).

The Dual Specificity Phosphatase 3 (DUSP3, also known as Vaccinia-H1 Related (VHR)), is part of the DUSP family, whose members dephosphorylate both threonine/serine and tyrosine residues (13,14). DUSP3 is a small protein of 185 amino acids encoded by the *DUSP3* gene located on chromosome 17q21 in humans and on chromosome 11 in mice (15). DUSP3 is highly expressed in endothelial cells, as well as in platelets and monocytes. It plays an essential role in the innate immune response, as well as in the regulation of cell adhesion and migration (16). DUSP3 modulates the cell cycle and inhibits various signaling pathways, including extracellular signal-regulated kinase 1/2 (ERK), signal transducer of activation 5 (STAT5) and epidermal

growth factor receptor (EGFR) (17). The role of DUSP3 in physiological and tumoral angiogenesis remains controversial. Full-body *Dusp3* knock-out (*Dusp3*$^{-/-}$) mice were generated, with no spontaneous phenotype (18). However, *Dusp3*$^{-/-}$ mice are resistant to LPS-induced endotoxemia and to polymicrobial septic shock induced by caecal ligation and perforation. Such protection seems to be macrophage-dependent, with a predominant shift towards an M2-like anti-inflammatory phenotype (19,20). The role of DUSP3 in "sterile" inflammation, such as the one observed *post* I/R, is unknown. In the present study, we investigate whether DUSP3 is present in the renal parenchyma and whether its genetic deletion in *Dusp3*$^{-/-}$ mice attenuates the I/R-associated inflammation and eventually participates in RIC.

Results

DUSP3 is expressed in the renal parenchyma and its abundance increases post renal I/R

An immune-reactive signal for DUSP3 was detected in podocytes (in co-localization with nephrin) and endothelial cells of glomeruli, as well as in Meca-32-positive endothelial cells of both the outer and inner medulla of mouse non-ischemic *WT* mouse kidneys (**Figure 1A**). No immunoreactivity for DUSP3 was detected in *Dusp3*$^{-/-}$ kidneys. Ten-week-old C57BL/6 *WT* (n=10) mice underwent unilateral left renal ischemia for 30 minutes. Right nephrectomy was simultaneously performed. Following renal reperfusion for 48h, the mRNA level of DUSP3 in the kidney was significantly increased (1.8-fold) compared to sham-operated condition ($p<0.001$) (**Figure 1B**). The renal abundance of DUSP3 protein was similarly increased *post* I/R (**Figure 1C**). Immunohistochemistry of DUSP3 on kidney specimens of *WT* and *DUSP3*$^{-/-}$ *post* I/R revealed an augmented expression in proximal tubules, endothelial cells and podocytes and, to a lesser extent, in distal tubules (**Figure 1D)**. These data suggest that DUSP3 may be involved in the pathophysiology of renal I/R injury.

Dusp3*$^{-/-}$ *mice are resistant to renal I/R injury

The comparative assessment of kidney function post-renal I/R showed that serum levels of urea (BUN) reached 78.4±33.7 *versus* 258.9±162.9 mg/dL in *Dusp3*$^{-/-}$ *versus WT* mice, respectively ($p<0.001$) (**Figure 2A**). BUN is a conventional biomarker of I/R-induced AKI. The Jablonski score of acute tubular necrosis on PAS-stained kidney sections was significantly lower in *Dusp3*$^{-/-}$ mice compared to controls ($p<0.05$) post-renal I/R **(Figure 2B)**. These functional and structural observations suggest that *Dusp3*$^{-/-}$ mice are less prone to renal I/R injury, which supports a role of DUSP3 in RIC.

Non-ischemic Dusp3*$^{-/-}$ *kidneys show an increased renal vascular density

In order to understand the mechanisms of the nephro-protection against I/R-induced AKI observed in *Dusp3*$^{-/-}$ mice, we investigated the renal vascularization of *Dusp3*$^{-/-}$ mice at baseline. At mRNA level, non-ischemic *Dusp3*$^{-/-}$ kidneys showed a significantly increased expression of Vascular Endothelial Growth Factor (VEGF) and Platelet endothelial cell adhesion molecule (PECAM1 or CD31), which are classical markers of angiogenesis, compared to controls ($p<0.01$) (**Figure 3A**). Furthermore, *Dusp3*$^{-/-}$ kidneys were characterized by a 1.8-fold increase in the

CD31-positive surface of the renal parenchyma compared to *WT* kidneys (11.56±1.07 *versus* 20.46±0.90; p<0.001) (**Figure 3B-C**). In line with these findings of an expanded renal vascular density, the renal resistivity index (RRI), non-invasively measured *in vivo* by kidney ultrasound, showed a decreased resistivity in the *Dusp3*$^{-/-}$ group (0.65±0.02 *versus* 0.57±0.03; p<0.01). (**Figure 3D-E**). Additionally, *Dusp3*$^{-/-}$ ischemic kidneys showed a significantly increased expression of VEGF at the mRNA level (p<0.01). (**Figure 3F**).

These observations suggest that the genetic inactivation of *Dusp3* favors renal angiogenesis, which may participate in RIC.

Phosphoproteomics indicate a down-regulation of inflammatory pathways and an up-regulation of angiogenesis, metabolism and transport in Dusp3*$^{-/-}$ *versus WT kidneys post-I/R

DUSP3 is a phosphatase which dephosphorylates both threonine/serine and tyrosine residues (14). In order to explore the pathways putatively involved in the RIC observed in *Dusp3*$^{-/-}$ mice, we performed hypothesis-independent phosphoproteomics, comparing *Dusp3*$^{-/-}$ and *WT* kidneys exposed to I/R. Among 24.856 peptides, 1.589 were found to be differentially expressed between the 2 groups. The sequence analysis of the preferred site for DUSP3, highlights, in particular, the preference for arginine at position -3 (**Figure 4A**). *Dusp3* deletion was associated with the down-regulation of phospho-sites involved in inflammation and with the up-regulation of phospho-sites implicated in the pathways of angiogenesis, metabolism and transport (**Figure 4B).**

On the basis of our initial observations of increased angiogenesis in *Dusp3*$^{-/-}$ kidneys, we first focused on the phosphorylation sites of pro-angiogenic factors. As summarized in **Table 1**, we found an increased phosphorylation of BASP1 and DLG1, which are well-established promoters of angiogenesis via the β-catenin and Dll4/Notch1 signaling pathways (28, 29). Most of the pro-angiogenetic factors found with increased phosphorylation levels in *Dusp3*$^{-/-}$ versus *WT* ischemic kidneys are involved in VEGF-mediated signaling: EPS8, FARP1, DOCK1, ARHGEF17, FARP2, IQGAP1, YY1, SIRT2, ARHGAP17, NDRG1 (30-36). Our phosphoproteomics-based observations suggest that the genetic inactivation of *Dusp3* may promote angiogenesis via the VEGF signaling pathway, which may in turn increase the vascular density and attenuate the I/R damage.

Kidney I/R typically alters cell metabolism (37). The enzymes classically involved in gluconeogenesis, like ALDO B, PCK1 and FBPase-1 (38), were found to be more phosphorylated in *Dusp3*$^{-/-}$ *versus WT* kidneys (**Table 2**). Such an augmented phosphorylation of gluconeogenic enzymes may be beneficial against renal I/R. Similarly, we observed an increased phosphorylation of mTOR and the glucocorticoid receptor in *Dusp3*$^{-/-}$ ischemic kidneys compared to WT, which suggests an increased metabolism in proximal and distal tubular epithelial cells, respectively. In line with these observations, we found several proximal tubular transporter and channels, such as AQP1, PKD, GLUT2, SGLT2, NHE3, NBC1, NaPi-IIa, and the amino acid transporter y^+-LAT1, y^+-LAT2 and $b(^{0,+})$-AT, to be significantly more phosphorylated in *Dusp3*$^{-/-}$ *versus WT* ischemic kidneys. Concerning the transporters of the distal tubule, NKCC2 and NHE3 were also found to be more phosphorylated (**Table 3**). Finally, the increased phosphorylation of the transcription factor PAX8 in *Dusp3*$^{-/-}$ ischemic kidneys may be interpreted as advantageous for tubular recovery *post* I/R (39).

Kidney I/R causes sterile inflammation, as mentioned above. Given the role of DUSP3 in the innate immune system, we finally focused on the phosphorylated proteins involved in inflammation (**Table 4**). *Dusp3* deletion was associated with the down-regulation of STAT3 and HGK *post* I/R, which have been reported as inducers of the c-Jun N-terminal kinase signaling pathway (JNK) through activating the MAP3K-MAP2K cascade (40). The JNK signaling pathway has been involved in I/R-induced AKI (41, 42). The phosphorylation status of c-Jun was confirmed to be lower in *Dusp3*$^{-/-}$ ischemic kidneys compared to *WT* by means of immunoblotting (**Figure 4C**). Similarly, the phospho-status of KIM-1, LSP1, and C/EBPβ, which are stimulating factors of inflammatory cell activation and migration (43-46), were significantly reduced, suggesting a reduced inflammation in *Dusp3*$^{-/-}$ ischemic kidneys compared to WT.

Dusp3*$^{-/-}$ *kidneys exposed to I/R show an attenuated inflammatory response

On the basis of these phosphoproteomics data, the expression of several actors of the inflammatory cascades was evaluated at both mRNA and protein levels in *WT* and *Dusp3*$^{-/-}$ mouse kidney samples post-I/R. Semi-quantification of mRNA levels of *interleukine-6 (IL-6)*, *CD11b*, *interleukine-1β (IL-1β)*, *caspase-3* and *TNF-α* showed that the increase of all of these transcripts due to I/R were attenuated by 4.15-fold ($p<0.001$), 1.9-fold ($p<0.001$), 2.3-fold ($p<0.001$), 2-fold ($p<0.05$) and 4-fold ($p<0.001$) in *Dusp3*$^{-/-}$ mice compared to *WT* samples, respectively (**Figure 5A**). The major difference observed between the two groups concerned (KIM-1) (43). KIM-1

mRNA level was 18-fold ($p<0.001$) less expressed in *Dusp3*$^{-/-}$ compared to *WT* kidneys. No difference in mRNA levels of these markers was observed between sham-operated *Dusp3*$^{-/-}$ and *WT* kidney (**Supplementary Figure IV-1**). At the protein level, the renal abundance of CD11b, PCNA and HSP70 was decreased 2.1-fold ($p<0.01$), 9.7-fold ($p<0.01$), and 2.7-fold ($p<0.001$) in *Dusp3*$^{-/-}$ kidney compared to controls conducted post-I/R, respectively. (**Figure 5B**). The counting of proliferating PCNA-positive cells at the cortico-medullary junction showed a 2.4-fold increase in *WT* compared to *Dusp3*$^{-/-}$ samples ($p<0.001$) *post* renal I/R. The number of F4-80-positive macrophages was similarly increased 1.7-fold in *WT* compared to *Dusp3*$^{-/-}$ kidneys ($p<0.001$). Finally, CD11b-positive cells were more numerous in *WT* compared to *Dusp3*$^{-/-}$ kidneys (3.5-fold, $p<0.001$) (**Figure 5C**). Of important note: no difference was observed between sham-operated *Dusp3*$^{-/-}$ and *WT* kidneys concerning the expression levels of PCNA, CD11b, and F4-80 (**Supplementary Figure IV-2**). In line with the phosphoproteomics analysis, these data suggest an attenuation of the inflammatory process in *Dusp3*$^{-/-}$ kidneys post-renal I/R.

Comparative analyses of urine and serum between wild-type and Dusp3*$^{-/-}$ *mice at baseline and after renal I/R

In order to refine the characterization of the phenotype observed in *Dusp3*$^{-/-}$ animals, we performed 24-hour urine collection for a comparative urinalysis of *WT* and *Dusp3*$^{-/-}$ mice (N=7 in each group) at baseline and after renal I/R. At baseline, the urine volume was not statistically different between groups, and no difference was observed between the two genotypes regarding urine levels of creatinine, α-1-microglobulin, albumin, Na^+, K^+, CL^-, and uric acid. Following I/R, the urinary levels of α-1-microglobulin and albumin were significantly higher in *WT* compared to *Dusp3*$^{-/-}$ animals ($p<0.05$) (**Table 5**). Additional blood analyses were carried out at baseline and after renal I/R. No difference was observed in baseline levels of serum creatinine (SCr), BUN, Na^+, K^+, Cl^- between genotypes. Following I/R, the levels of SCr and BUN were significantly lower in *Dusp3*$^{-/-}$ *post* I/R compared to *WT post* I/R ($p<0.05$). GFR was significantly reduced in *WT post* I/R compared to *Dusp3*$^{-/-}$ *post* I/R ($p<0.05$) (**Table 6**).

Discussion

The pathophysiology of I/R-induced AKI is complex, which hampers the development and validation of innovative therapeutic approaches (5,37,46,47). Our observations suggest that the whole-body genetic deletion of *Dusp3* in mice, is protective against renal I/R, with maintained kidney function and architecture, attenuated inflammation and preserved cell metabolism. The M2 anti-inflammatory macrophage response was upregulated in *Dusp3*$^{-/-}$ mice, in line with previous reports involving DUSP3 in the regulation of the innate immune response (48,49). The renal induction of M2 macrophages has been shown to preserve kidney function and architecture in models of I/R injury (50,51). Conversely, an overwhelmed innate immune response with a secretory burst of cytokines and interleukins, like IL-6 and TNFα, inevitably accelerates the worsening of kidney damage post-renal I/R (52,53). Balancing the signaling pathways downstream of the I/R cascade may help attenuate the renal injury (54).

In addition to the inflammation and recruitment of inflammatory cells, the early stages of renal I/R involve an anti-angiogenic response, whereas prolonged hypoxia at later stages *post* renal I/R, activates pro-angiogenic factors (55). Such a sequential response may help stabilize the renal microvasculature and favor the local blood supply, as observed in surgery-induced RIC (55, 11, and 12). The quantification of the CD31–positive vascular network in the renal parenchyma of *Dusp3*$^{-/-}$ mice compared to *WT* littermates at baseline, showed a significantly increased vascular density in the absence of DUSP3. Furthermore, ischemic *Dusp3*$^{-/-}$ kidneys showed significantly increased mRNA expression levels of VEGF, which may mirror the RIC observed in *Dusp3*$^{-/-}$ mice. The role of DUSP3 in angiogenesis is debatable. On the one hand, DUSP3 may be pro-angiogenic by affecting the β-FGF-induced endothelial cell sprouting, probably via the PKC pathway, as suggested in a matrigel-based angiogenesis assay (18). On the other hand, *Dusp3* deletion has been shown to increase vascularity in an experimental metastasis model using *Lewis* lung carcinoma cells (21). In our study, the renal resistivity index, measured *in vivo* by ultrasound,

showed a decreased resistivity in the *Dusp3*$^{-/-}$ group, which further supports an enhanced renal vascularization. In order to decipher how DUSP3 may modulate I/R-induced pathways, phospho-proteomics was used and highlighted increased phosphorylation of pro-angiogenic factors, in particular, those involved in VEGF-mediated signaling in *Dusp3*$^{-/-}$ ischemic kidneys. Similarly, we have observed an increased phosphorylation of well-known metabolic enzymes, transporters and channels of both proximal and distal tubules in *Dusp3*$^{-/-}$ versus *WT* ischemic kidneys, which is in congruent with augmented DUSP3 expression in WT proximal and distal tubules following I/R. Proximal tubular cells are sensitive to IR-induced injury leading to several alterations, including brush-border membrane disruption, loss of cell polarity, loss of tight junctions and reduced transcellular transport capacity for metabolites (56). The reduction in transporter activity upon I/R were shown to affect renal and whole-body homeostasis, as well as detoxification processes and xenobiotic clearance (56). In our study, phosphoproteomic analysis revealed increased phosphorylation of SGLT2 and GLUT-2 for glucose transport, NHE3 and NKCC2 for sodium transport, AQP1 and AQP2 for transcellular water transport and various amino acid transporters, although the consequences of phosphorylation on the respective site remain unknown for most of the identified sites. In congruence with augmented transporter phosphorylation, increased mammalian homolog of TOR1 (mTORC), AMP-activated kinase (AMPK) and various protein kinase C (PKC) and ribosomal S6 protein kinase delta 1 (RSKL1, downstream signaling of mTORC1) phosphorylation occurred. It is a well-acknowledged fact that mTORC1 is the main kinase-regulating proximal tubular transport (57) including SGLT2, Napi-IIa and most of the amino acid transporter, which our study showed to have increased. Similarly, in the kidney, AMPK interferes with sodium handling by activating NKA, NKCC2 and promotes glucose uptake indirectly by activating basolateral GLUT-2 (58). In line with augmented SGLT2 and GLUT-2 phosphorylation in DUSP3 $^{-/-}$ kidneys post I/R compared to WT post I/R, two major enzymes for gluconeogenesis phosphoenolpyruvate carboxykinase (PCK1, PEPCK) and fructose-1, 6-bisphospahatse (FBPase) demonstrated an increased level of phosphorylation as well. Augmented phosphorylation, together with preserved kidney function, suggests that increased tubular functions in *DUSP3*$^{-/-}$ vs. *WT post I/R* occurs upon inhibition of DUSP3-induced dephosphorylation. Analysis in intensive care unit patients revealed that AKI correlated with high lactate and low glucose levels (59). Furthermore, AKI-associated mortality was shown to be restricted to patients with higher lactate and lower glucose levels and metabolic function of renal tubules was therefore suggested to affect the whole body, and finally, the critical illness and

mortality of patients. Together, DUSP3 deletion-induced increased phosphorylation levels of various transporters, kinases and enzymes for gluconeogenesis may additionally preserve renal and whole body functions leading to a better clinical outcome after ischemia induced injury.

In addition, we have observed a down-regulation of inflammatory factors, in particular the JNK signaling pathway, in *Dusp3*$^{-/-}$ *versus WT* ischemic kidneys. c-Jun has been previously involved in AKI induction post-I/R (41, 42). JNK inhibition has also been shown to provide significant protection against aristolochic acid-induced AKI (60).

Altogether, our observations indicate that DUSP3 may play a role in renal angiogenesis and in the modulation of sterile inflammation following renal I/R. The functional loss of DUSP3 appears nephro-protective in the case of I/R-induced AKI. Pharmacological inhibitors of DUSP3 are under development, although none of them is available *in vivo* yet (61,62). A DUSP3 drug-targeting strategy may pave the way for innovative therapeutics in the field of renal I/R.

The development and validation of DUSP3 inhibitors for pharmaceutical intervention before I/R may help to simultaneously improve multiple major pathophysiological processes involved in the ischemic cascade, including renal hemodynamics, production of inflammatory cytokines, endothelial and tubular cell injury and whole body metabolism.

Materials and methods

Mouse model of renal I/R. The Institutional Animal Care and Use Committee of the University of Liege approved the present protocol (#1335). The generation of *Dusp3*$^{-/-}$ mice (in C57BL/6-CD45.2 background) has been described previously (21). All breeding and genotyping were performed at the ULiege animal facility as previously reported (21). Wild-type (*WT*) mice are C57BL/6-CD45.2 littermates of *Dusp3*$^{-/-}$. All mice were housed in ventilated cages under conditions of stable temperature (23°C) and humidity under dark/light cycle, with *ad libitum* access to food and water. All recordings/analyses were carried out by investigators who were blinded to the experimental conditions. Male mice aged 8-10 weeks (~26g) were anesthetized with pentobarbital (60mg/kg). Analgesia was performed preoperatively using buprenorphine (0.05mg/kg). Median laparotomy was performed on heating pads, and a vascular clamp was applied for 30 minutes on the left renal pedicle. The right kidney was removed during the ischemia period and was half-cut to be fixed in paraformaldehyde or snap-frozen in liquid nitrogen. During the laparotomy, mice were covered with moistened gauze, saline solution (0.5mL/100g) and antibiotics (Enrofloxacin 2.5%, 0.025mL/mice) were intraperitoneally infused. After surgery, mice were monitored twice daily. The left kidney was reperfused for 48 hours. Then, the mice were anesthetized. A blood sample was collected by puncture of the inferior vena cava and centrifuged at 100 g for 5min at 4°C. The serum level of blood urea nitrogen (BUN) was measured by enzymatic methods (Roche/Hitachi Cobas). The left kidney was excised, half-cut, and fixed in paraformaldehyde or snap-frozen in liquid nitrogen.

Ultrasound-based assessment of renal resistivity index. Male mice (aged between 14-25 weeks) were anesthetized with 4% isoflurane and kept in a sleep state by 1.5% isoflurane. Renal Doppler ultrasound was performed by a certified-board vet (GB) using a HITACHI ARIETTA 850 SE ultrasound system equipped with a Broadband Linear Array Transducer with an 18-5 MHz extended frequency range. The investigator was blinded to the genotype. Renal Doppler blood flow was obtained by taking the mean value of 3 different evaluations guided by color-flow mapping: peripheral arteries, meso-renal arteries, and renal artery from kidneys. The measured parameters were peak-systolic velocity (PSV), end-diastolic velocity (EDV), and renal resistive index (RRI). PSV and EDV are expressed as cm/s. RRI was calculated as (PSV-EDV)/PSV.

Histology and immunostaining. Kidney tissues were fixed in paraformaldehyde for 24 hours and then embedded in paraffin. Kidney Sections (5-µm) were dewaxed and gradually hydrated before hematoxylin-eosin (HE) and Periodic Acid Schiff (PAS) staining. I/R-induced acute tubular necrosis (ATN) was blindly scored following the Jablonski score. For immunohistochemistry (IHC), sections were subjected to antigen retrieval in sodium citrate buffer (pH 6.0, Dako #S2031) or Target buffer (Dako #S1699) or EDTA buffer (Dako #S2367). Endogenous peroxidase activity was blocked with 3% hydrogen peroxide (Merck 30%, #107209) for 20 minutes at RT. Non-specific binding was constrained by incubation for 30min with either normal goat serum or for 10min with protein block reagent (Dako #X0909). Then, sections were incubated for 60min at RT with primary antibodies: monoclonal mouse anti-PCNA (Dako, #M0879 1/2500); anti-F4/80 (Abcam #74383 1/1000); anti-CD11b (Abcam, #7546 1/6000) and anti-CD31 antibodies (Abcam #28364 1/200) were used. After washing, sections were incubated for 30min with goat anti-mouse or rabbit biotin-conjugated secondary antibodies (Envision anti-Rabbit/HRP, Dako #K4003 1/400), washed and exposed to horseradish peroxidase-conjugated streptavidin (1/500) for 30min. Immunoreactivity was detected using DAB (Dako #K3468) or AEC (Dako #K3464). IHC scoring was achieved blindly: 4 randomly selected fields of the cortico-medullary region (magnification, 20x) were assessed per kidney. Staining was reported to the global number of cells in the considered area (i.e. per cells/mm^2). CD31 immunostaining was quantified blindly on digital images (NanoZoomer 2.0 HT, Hamamatsu®). Using the particle plug-in for vascular density on the Fiji program (version 1.52i; Wayne Rasban, NIH), the images were processed by color deconvolution using a set of macros instruction. The color deconvolution separates the image to isolate the signal from the histological dyes (DAB staining signal), which marks the vessels. A constant threshold was used to exclude the background for all images. The percentage area obtained was defined as a percentage of the area of CD31-positive vessels (white pixels) to the total area of the slice. The following formula was used to calculate vascular density: vascular density = vessel area/total area*100%.

Immunofluorescence. Paraffin sections were subjected to antigen retrieval in a sodium citrate buffer (pH 6.0), blocked with 5% skim milk/PBS and incubated with rabbit anti-DUSP3 (Abcam) and either with rat anti-Meca32 (Novus), guinea pig anti-nephrin (GP-N2, Progen) or guinea pig anti-megalin (63) overnight followed by a suitable Alexa488 or Alexa555-coupled secondary

antibody (Dianova, Hamburg). The double-antibody staining procedure was controlled by parallel incubation of consecutive sections, each probed only with a single antibody. Sections were analyzed using a multilaser confocal scanning microscope (Abberior, Facility Line).

Immunoblotting. Half-kidneys were grinded and homogenized by oscillations (Mikrodismembrator S, B. Braun Biotek International) for 1 minute at 2.500 rpm. Protein extraction was performed using ice-cold TEN-T buffer, including protease and phosphatase inhibitors (Roche®), until complete solubilization of the renal powder. Supernatant was collected after centrifugation at 13.000rpm for 30min at 4°C. The Bradford method was used to determine protein concentration. Protein lysates were mixed with Laemmli buffer (1:4) and heated for 2 minutes at 95°C. Samples were loaded and separated at 100V on stain-free SDS gel electrophoresis gels (Bio-Rad®) (20µg/lane). Gels were exposed to UV light for 5min (ChemiDoc MP System, Bio-Rad®). Proteins were transferred to PVDF membranes using the Trans-Blot Turbo Transfer System for 7 or 5 minutes at RT depending on the molecular weight of the targeted protein. Blots were blocked with 5% milk in Trisbuffered saline with Tween 20 (TBS-T) for 1h and incubated overnight at 4°C with primary antibodies: anti-DUSP3 (Cell Signaling Technology #4752 1/1000), anti-CD11b (Abcam #ab7546 1/1000), anti-HSP70 (Enzo #810F 1/1000) and anti-PCNA (Dako #M0879 1/1000). Blots were rinsed five times with TBS-T for 5min, and incubated with appropriate HRP-conjugated anti-rabbit or anti-mouse secondary antibodies (1/4.000) for 90 minutes at RT. After rinsing 5 times for 5min each, chemiluminescent signals were captured using chemiluminescent substrate (SuperSignal West Femto Maximum Sensitivity Substrate, Thermoscientific®), and detected by the ChemiDoc MP System. Immunoreactive signals were quantified using Bio-Rad® stain-free technology after normalization to total protein content. Anti-P-c-Jun (Ser63) (Cell signaling #2361 1/1000) was used for Phospho-c-Jun (P-c-Jun) immunoblotting with a Rab11 (D4F5) XP® (Cell signaling #5589 1/2000) loading control. Anti-rabbit IgG (H+L) (DyLight™ 680 Conjugate) was used as a secondary antibody (Cell signaling #5366 1/10000). Immunoreactive signal was visualized by LiCOR®, and quantified after normalization to loading control.

Real-time semi-quantitative polymerase chain reaction (RT-qPCR). Fifty mg of kidney powder were homogenized in 1mL NucleoZOL solution (Macherey-Nagel®) + 400µL of RNase-free water and incubated at RT for 10minutes. Lysates were centrifuged at 12.000 g at 4°C for 15min. One

mL of supernatant was transferred to a fresh RNase-free tube and 1mL of isopropanol 100% was added to precipitate RNA. The mixtures were centrifuged at 12.000 g at 4°C for 10min, and RNA pellets were washed 2 times with 500µL of 75% ethanol before centrifugation at 6000g at 4°C for 3min. Pellets were finally dissolved in 100µL RNase-free water. RNA concentration and purity were assessed using a NanoDrop Lite spectrophotometer (Thermo Scientific®). All RNA samples had an absorbance [260nm/280nm] ratio comprised between 1.8 and 2.2. Following this, cDNAs were generated using Reverse Transcription Kit (Promega®) according to manufacturer's instruction. Primers used for RT-qPCR are listed in **Supplementary Table I**. Semi-quantitative mRNA expression levels were calculated using threshold cycle (Ct) values following the classical $2^{-\Delta CT}$ equation. The housekeeping gene used for RT-qPCR was *Gapdh*.

Urine collection apparatus

The metabolic cage (Nalgene, Thermo Fisher) designed specifically for mice features a unique funnel and cone design that effectively separates feces and urine into tubes outside the cage. This cage is designed to allow for immediate, complete and total separation of urine and feces. The usable floor area is 200 cm^2 with an internal height of 130 mm.

Dusp3$^{-/-}$ and *WT* mice were individually housed in the metabolic cage for 24h and immediately returned to pair housing in their home cages at the end of the session. The animals underwent one habituation session in the cage beforehand with the same duration. Mice had free access to water and food. All cages were cleaned thoroughly with detergents (Contrex, Decon Labs, King of Prussia, PA) and water between sessions. For technical and ethical reasons, blood puncture and analysis at the baseline were performed in littermates of the *Dusp3*$^{-/-}$ and *WT* mice used for I/R. Urea, creatinine, albumin, α-1-microglobulin, Na^+, K^+, Cl^-, Ca^{2+} and uric acid levels in urine or serum were measured using the AU480 chemistry analyzer (Beckman Coulter, Brea, California, United States). The following formulas were used to calculate the Glomerular filtration rate (GFR): GFR= [(urine creatinine (mmol/l) x urine volume (µl)) / (plasma creatinine (mmol/l) x 1440 min)], and Fractional Excretion of Sodium (FeNa): FeNa= [(urine Na^+ / plasma Na^+) / (urine creatinine/plasma creatinine)] x 100.

IMAC enrichment of phosphopeptides (Fe-IMAC)*:*

Powders of mouse kidney post-I/R were prepared with 6 biological replicates of *WT* and *Dusp3*$^{-/-}$ condition and shipped to Cell Signaling Technology (Danvers, USA) for analysis. Tissue powders were solubilized in Urea Lysis Buffer (9M Urea, 20mM HEPES pH 8.0 + phosphatase inhibitor cocktail) and were sonicated and centrifuged to remove insoluble material. Equal protein quantities from 3 replicates each were combined to create 4 final samples, 2 for *WT* and 2 for *Dusp3*$^{-/-}$. Samples were reduced with DTT and alkylated with iodoacetamide. 500µg total protein for each sample was digested with trypsin, purified over C18 columns (Waters) and used for IMAC enrichment using Fe-NTA magnetic beads (CST #20432) as previously described (22). LC-MS/MS analysis was performed using a Thermo Orbitrap Fusion™ Lumos™ Tribrid™ mass spectrometer as previously described (22, 23) with replicate injections of each sample. Briefly, peptides were separated using a 50cm x 100µM PicoFrit capillary column packed with C18 reversed-phase resin and eluted with a 150-minute linear gradient of acetonitrile in 0.125% formic acid delivered at 280nl/min. Tandem mass spectra were collected in a data-dependent manner by using a top-twenty MS/MS method, a dynamic repeat count of one, and a repeat duration of 30 sec. Real time recalibration of mass error was performed using lock mass (24) with a singly charged polysiloxane ion m/z = 371.101237**.** MS spectra were evaluated by Cell Signaling Technology using Comet and the GFY-Core platform (Harvard University) (25). Searches were performed against the most recent update of the Uniprot *Mus musculus* database with a mass accuracy of +/-20 ppm for precursor ions and 0.02 Da for product ions. Results were filtered to a 1% peptide-level FDR with mass accuracy +/-5 ppm on precursor ions and presence of a phosphorylated residue for IMAC enriched samples. All IMAC quantitative results were generated using Skyline (26) to extract the integrated peak area of the corresponding peptide assignments. Accuracy of quantitative data was ensured by manual review in Skyline or in the ion chromatogram files. To generate sequence logos, we used the plogo tool (27), all phosphopeptides identified in the study were used as the background and the subset of peptides that increased in abundance with *Dusp3*$^{-/-}$ were used as the test set. -7/+7 sequences were used as the input with the phosphorylation site centered.

Statistical analyses. Data were expressed as mean ± standard deviation (SD). Data normality was measured using 4 normality test (D'Agostino-Pearson, Anderson-Darling, Shapiro-Wilk and Kolmogorov-Smirnov). The unpaired parametric T-test was used in the case where normality test was passed and unpaired nonparametric test (Mann-Whitney) was used in the case where

normality test was not passed. Chi-square test were used to compare discrete variables, with a p-value ≤ 0.05 as the statistically significant threshold. Analysis of data was performed using GraphPad PRISM software (GraphPad Software, La Jolla, CA).

Acknowledgments

FJ is a Fellow of the Fonds National de la Recherche Scientifique (FNRS) and received support from the University of Liège (*Fonds Spéciaux à la Recherche, Fonds Léon Fredericq*) and the FNRS (Research Credits 2013 and 2016). FT was supported by the DFG (CRC 877) and Helmut Horten Foundation. The authors acknowledge Kathryn Abell (Cell Signaling) for technical assistance.

Funding: *Fonds National de la Recherche Scientifique* (FNRS), Belgium; German Research Foundation (DFG)

Competing Financial Interests

All the authors declared no competing interests.

Sample statement

The data that support the findings of this study are available from the corresponding author upon reasonable request.

References

1. Hoste EA, Kellum JA, Selby NM et al. Global epidemiology and outcomes of acute kidney injury. Nature Reviews Nephrology 2018; 14: 607–625.
2. Bonventre JJ V, Yang L. Cellular pathophysiology of ischemic acute kidney injury. The Journal of clinical investigation 2011; 121: 4210–4221.
3. Rowart P, Erpicum P, Detry O et al. Mesenchymal Stromal Cell Therapy in Ischemia/Reperfusion Injury. Journal of Immunology Research 2015; 2015.
4. Erpicum P, Rowart P, Poma L, Krzesinski J-M, Detry O, Jouret F. Administration of mesenchymal stromal cells before renal ischemia/reperfusion attenuates kidney injury and may modulate renal lipid metabolism in rats. Scientific Reports 2017; 7: 8687.
5. Kalogeris T, Baines CP, Krenz M, Korthuis RJ. Cell biology of ischemia/reperfusion injury. International Review of Cell and Molecular Biology 2012; 298: 229–317.
6. Shen H, Kreisel D, Goldstein DR. Processes of Sterile Inflammation. The Journal of Immunology 2013; 191: 2857–2863.
7. Kvietys PR, Granger DN. Role of reactive oxygen and nitrogen species in the vascular responses to inflammation. Free Radical Biology and Medicine 2012; 52: 556–592.
8. Denecke C, Tullius SG. Innate and adaptive immune responses subsequent to ischemia-reperfusion injury in the kidney. Progrès en Urologie 2014; 24: S13--S19.
9. Chiba T, Cerqueira DM, Li Y et al. Endothelial-Derived miR-17~92 Promotes Angiogenesis to Protect against Renal Ischemia-Reperfusion Injury. JASN 2021; 32:553-562.
10. Wang Y, Mi Y, Tian J et al. Intermedin Alleviates Renal Ischemia-Reperfusion Injury and Enhances Neovascularization in Wistar Rats. Drug Des Devel Ther 2020; 14:4825-4834.
11. Erpicum P, Detry O, Weekers L et al. Mesenchymal stromal cell therapy in conditions of renal ischaemia/reperfusion. Nephrology Dialysis Transplantation 2014; 29: 1487–1493.
12. Wever KE, Menting TP, Rovers M et al. Ischemic preconditioning in the animal kidney, a systematic review and meta-analysis. PLoS One 2012; 7:e32296.
13. Schumacher MA, Todd JL, Rice AE, Tanner KG, Denu JM. Structural Basis for the Recognition of a Bisphosphorylated MAP Kinase Peptide by Human VHR Protein Phosphatase. Biochemistry 2002; 41: 3009–3017.

14. Huang C-Y, Tan T-H. DUSPs, to MAP kinases and beyond. Cell & Bioscience 2012; 2: 24.
15. Ishibashi T, Bottaro DP, Chan A, Miki T, Aaronson SA. Expression cloning of a human dual-specificity phosphatase. Proceedings of the National Academy of Sciences of the United States of America 1992; 89: 12170–12174.
16. Pavic K, Duan G, Köhn M. VHR/DUSP3 phosphatase: structure, function and regulation. The FEBS Journal 2015; 282: 1871–1890.
17. Alonso A, Saxena M, Williams S, Mustelin T. Inhibitory role for dual specificity phosphatase VHR in T cell antigen receptor and CD28-induced Erk and Jnk activation. Journal of Biological Chemistry 2001; 276: 4766–4771.
18. Amand M, Erpicum C, Bajou K et al. DUSP3/VHR is a pro-angiogenic atypical dual-specificity phosphatase. Molecular Cancer 2014; 13: 1–18.
19. Singh P, Dejager L, Amand M et al. DUSP3 Genetic Deletion Confers M2-like Macrophage-Dependent Tolerance to Septic Shock. Journal of Imunology 2015; 194: 4951–4962.
20. Vandereyken MM, Singh P, Wathieu CP et al. Dual-Specificity Phosphatase 3 Deletion Protects Female, but Not Male, Mice from Endotoxemia-Induced and Polymicrobial-Induced Septic Shock. Journal of Immunology 2017; 199: 2515–2527.
21. Vandereyken M, Jacques S, Overmeire E Van et al. Dusp3 deletion in mice promotes experimental lung tumour metastasis in a macrophage dependent manner. PLoS ONE 2017; 1: 1–23. 21.
22. Stokes MP, Farnsworth CL, Gu H et al. Complementary PTM Profiling of Drug Response in Human Gastric Carcinoma by Immunoaffinity and IMAC Methods with Total Proteome Analysis. Proteomes 2015; 3: 160-183.
23. Possemato AP, Paulo JA, Mulhern D et al. Multiplexed Phosphoproteomic Profiling Using Titanium Dioxide and Immunoaffinity Enrichments Reveals Complementary Phosphorylation Events. J Proteome Res 2017; 16:1506-1514.
24. Olsen JV, de Godoy LM, Li G et al. Parts per million mass accuracy on an Orbitrap mass spectrometer via lock mass injection into a C-trap. Mol Cell Proteomics 2005; 4:2010-2021.
25. Huttlin EL, Jedrychowski MP, Elias JE et al. A tissue-specific atlas of mouse protein phosphorylation and expression. Cell 2010; 143:1174-1189.
26. MacLean B, Tomazela DM, Shulman N et al. Skyline: an open source document editor for

creating and analyzing targeted proteomics experiments. Bioinformatics 2010; 26:966-8.
27. O'Shea JP, Chou MF, Quader SA et al. pLogo: A probabilistic approach to visualizing sequence motifs. Nat Methods 2013; 10:1211-1212.
28. Khajavi M, Zhou Y, Schiffer AJ et al. Identification of Basp1 as a novel angiogenesis-regulating gene by multi-model system studies. FASEB J 2021; 35:e21404.
29. Cho C, Wang Y, Smallwood PM et al. Dlg1 activates beta-catenin signaling to regulate retinal angiogenesis and the blood-retina and blood-brain barriers. Elife 2019; 8:e45542.
30. Cappellini E, Vanetti C, Vicentini LM et al. Silencing of Eps8 inhibits in vitro angiogenesis. Life Sci 2015; 131:30-6.
31. Hernández-García R, Iruela-Arispe ML, Reyes-Cruz G et al. Endothelial RhoGEFs: A systematic analysis of their expression profiles in VEGF-stimulated and tumor endothelial cells. Vascul Pharmacol 2015; 74:60-72.
32. Wang H, Ramshekar A, Kunz E et al. IQGAP1 causes choroidal neovascularization by sustaining VEGFR2-mediated Rac1 activation. Angiogenesis 2020; 23:685-698.
33. Liu H, Qiu Y, Pei X et al. Endothelial specific YY1 deletion restricts tumor angiogenesis and tumor growth. Sci Rep 2020; 10:20493.
34. Hu F, Sun X, Li G et al. Inhibition of SIRT2 limits tumour angiogenesis via inactivation of the STAT3/VEGFA signalling pathway. Cell Death Dis 2018; 10:9.
35. Kiso M, Tanaka S, Saji S et al. Long isoform of VEGF stimulates cell migration of breast cancer by filopodia formation via NRP1/ARHGAP17/Cdc42 regulatory network. Int J Cancer 2018. 143:2905-2918.
36. Watari K, Shibata T, Fujita H et al. NDRG1 activates VEGF-A-induced angiogenesis through PLCγ1/ERK signaling in mouse vascular endothelial cells. Commun Biol 2020; 3:107.
37. Erpicum P, Rowart P, Defraigne J-O, Krzesinski J-M, Jouret F. What we need to know about lipid-associated injury in case of renal ischemia-reperfusion. American Journal of Physiology - Renal Physiology 2018; 315.
38. Yañez AJ, Ludwig HC, Bertinat R et al. Different involvement for aldolase isoenzymes in kidney glucose metabolism: aldolase B but not aldolase A colocalizes and forms a complex with FBPase. J Cell Physiol 2005;202:743-53.
39. Sharma R, Sanchez-Ferras O, Bouchard M. Pax genes in renal development, disease and regeneration. Semin Cell Dev Biol 2015; 44:97-106.

40. Yao Z, Zhou G, Wang XS et al. A novel human STE20-related protein kinase, HGK, that specifically activates the c-Jun N-terminal kinase signaling pathway. J Biol Chem 1999; 274:2118-25.
41. Kaushal GP, Shah S V. Challenges and advances in the treatment of AKI. Journal of the American Society of Nephrology 2014; 25: 877–883.
42. Kanellis J, Ma FY, Kandane-Rathnayake R et al. JNK signalling in human and experimental renal ischaemia/reperfusion injury. Nephrol Dial Transplant 2010; 25: 2898–2908
43. Han WK, Bailly V, Abichandani R, Thadhani R, Bonventre J V. Kidney Injury Molecule-1 (KIM-1): A novel biomarker for human renal proximal tubule injury. Kidney International 2002; 62: 237–244
44. Tian L, Shao X, Xie Y et al. Kidney Injury Molecule-1 is Elevated in Nephropathy and Mediates Macrophage Activation via the Mapk Signalling Pathway. Cell Physiol Biochem 2017; 41:769-783.
45. Jongstra-Bilen J, Jongstra J. Leukocyte-specific protein 1 (LSP1): a regulator of leukocyte emigration in inflammation. Immunol Res 2006; 35:65-74.
46. Yang X, Qi F, Wei S et al. The Transcription Factor C/EBPβ Promotes HFL-1 Cell Migration, Proliferation, and Inflammation by Activating lncRNA HAS2-AS1 in Hypoxia. Front Cell Dev Biol 2021; 9:651913.
47. Tögel FE, Westenfelder C. Mesenchymal stem cells: a new therapeutic tool for AKI. Nature Reviews Nephrology 2010; 6: 179–183.
48. Russo LC, Farias JO, Ferruzo PYM, Monteiro LF, Forti FL. Revisiting the roles of VHR/DUSP3 phosphatase in human diseases. Clinics 2018; 73: 1–7.
49. Monteiro LF, Ferruzo PYM, Russo LC, Farias JO, Forti FL. DUSP3/VHR: A druggable dual phosphatase for human diseases. Reviews of Physiology, Biochemistry and Pharmacology 2019; 176: 1–35.
50. Alikhan MA, Jones C V., Williams TM et al. Colony-stimulating factor-1 promotes kidney growth and repair via alteration of macrophage responses. American Journal of Pathology 2011; 179: 1243–1256.
51. Huen SC, Cantley LG. Macrophage-mediated injury and repair after ischemic kidney injury. Pediatric Nephrology 2015; 30: 199–209.
52. Kezić A, Stajic N, Thaiss F. Innate Immune Response in Kidney Ischemia/Reperfusion Injury: Potential Target for Therapy. Journal of Imunology Research 2017; 2017: 1–10.

53. Slegtenhorst BR, Dor FJ, Rodriguez H, Voskuil FJ, Tullius SG. Ischemia/reperfusion Injury and its Consequences on Immunity and Inflammation. Current Transplantation Reports 2014; 1: 147–154.
54. Lang R, Raffi FAM. Dual-specificity phosphatases in immunity and infection: An update. International Journal of Molecular Sciences2019; 20.
55. Pallet N, Thervet E, Timsit MO. Angiogenic response following renal ischemia reperfusion injury: New players. Progres en Urologie 2014; 24.
56. Faucher Q, Alarcan H, Marquet P, Barin-Le Guellec C. Effects of Ischemia-Reperfusion on Tubular Cell Membrane Transporters and Consequences in Kidney Transplantation. J Clin Med 2020; 9:2610.
57. Grahammer F, Ramakrishnan SK, Rinschen MM et al. mTOR Regulates Endocytosis and Nutrient Transport in Proximal Tubular Cells. J Am Soc Nephrol. 2017; 28:230-241.
58. Juszczak F, Caron N, Mathew AV, Declèves AE. Critical Role for AMPK in Metabolic Disease-Induced Chronic Kidney Disease. Int J Mol Sci. 2020; 21:7994.
59. Legouis D, Ricksten SE, Faivre A et al. Altered proximal tubular cell glucose metabolism during acute kidney injury is associated with mortality. Nat Metab. 2020; 2:732-743.
60. Fan Y, Elyce O, Frank Y et al. c-Jun Amino Terminal Kinase Signaling Promotes Aristolochic Acid-Induced Acute Kidney Injury. Front Physiol 2021; 12:599114.
61. Shi Z, Tabassum S, Jiang W et al. Identification of a Potent Inhibitor of Human Dual-Specific Phosphatase, VHR, from Computer-Aided and NMR-Based Screening to Cellular Effects. ChemBioChem 2007; 8: 2092–2099.
62. Wu S, Vossius S, Rahmouni S et al. Multidentate Small-Molecule Inhibitors of VacciniaH1-Related (VHR) Phosphatase Decrease Proliferation of Cervix Cancer Cells. Journal of Medicinal Chemistry 2009; 52: 6716–6723.
63. Grahammer F, Ramakrishnan SK, Rinschen MM et al. mTOR Regulates Endocytosis and Nutrient Transport in Proximal Tubular Cells. J Am Soc Nephrol. 2017 ; 28:230-241.

Phospho-sites tables from Fe-IMAC analysis:

Table 1:

Angiogenesis	Protein Name	Fold change DUSP3-KO/WT	AA-site
brain acid-soluble protein 1	BASP1	+5.4	36
Disks large homolog 1	DLG1	+3,2 +3,1 +2,7 +2,5 +6,7 +2,7	673;707 676;688;710 678;690;712 415;448;448 484;517;517 682;694;716
Epidermal growth factor receptor kinase substrate 8	EPS8	+3,2 +2,6	658;661 109
Adaptor protein NCK1	NCK1	+2.9	89
Paxillin	PXN	+2,9 +3,1 +3,4 +2,9 +2,9	303 126;130;126;130 132;132 136;136 137;137
FERM, ARHGEF and pleckstrin domain-containing protein 1	FARP1	+3,2 +3,2 +3,2 +3,1 +3,2	403 881; 892 892;899 902 396
Dedicator of cytokinesis protein 1	DOCK1	+16.5	1704
Ras GTPase-activating-like protein IQGAP1	IQGAP1	+3.1	1097
Myristoylated alanine-rich C-kinase substrate	MARCKS	+3.6	141
Rap1 GTPase-activating protein 1	RAPGAP1	+3.6	601;602;537;538;539;568;569;570;
Stromal interaction molecule 1	STIM1	+5.1	504
Secretogranin-2	SCG2	+2.5	532;533;556
FERM, ARHGEF and pleckstrin domain-containing protein 2	FARP2	+3.1	401;406
Transcriptional repressor protein YY1	YY1	+3.1	247
NAD-dependent protein deacetylase sirtuin-2	SIRT2	+2.6	368;331;298 372;335;302
Rho GTPase-activating protein 17	ARHGAP17	+5,3 +3,9	162 671;593;
Rho guanine nucleotide exchange factor 17	ARHGEF17	+2.5	921;922
Caveolae-associated protein 2	CAVIN2	+3.7	27; 32
N-myc downstream regulated gene 1	NDRG1	+2,5 +2,5	333, 336 336
Nuclear Receptor Coactivator SRC-3	SRC-3	+6,4	720

Table 2:

Metabolism	Protein name	Fold change DUSP3-KO/WT	AA-site
Fructose-bisphosphate aldolase B	ALDOB	+2,6 +2,9 +2,9	272 276 281
Phosphoenolpyruvate carboxykinase, cytosolic [GTP]	PCK1	+3.4	286
Fructose-1,6-bisphosphatase 1	FBPase-1	+3.5 +3.5	297 298
5'-AMP-activated protein kinase subunit beta-1 5'-AMP-activated protein kinase subunit beta-2 5'-AMP-activated protein kinase subunit gamma-2	AMPKB1 AMPKB2 AMPKG1	+4.0 +4.2 +3.5 +3.2 +3.2	106 108 107 109 113
Serine/threonine-protein kinase mTOR	mTOR	+5,7 +2,7	2448 2454
Ribosomal protein S6 kinase delta-1	RSKL1	+2.9	779;697;748
Glucocorticoid receptor	GR	+3,5 +3,5	412;385; 411;384;
Paired box protein Pax-8	PAX8	+3,6	252

Table 3:

Channels and transporter	Protein name	Fold change DUSP3-KO/WT	AA-site
Aquaporin-1	AQP1	+3.9	262
Extracellular calcium-sensing receptor	CaR	+2,5 +2,7 +3,6	1062;985 875;798 1004;927
Polycystin-2	PKD2	+3.4	806, 810;750, 754
Solute carrier family 12 member 1	NKCC2	+4,1 +3,9	116 28
Solute carrier family 2, facilitated glucose transporter member 2	GLUT2	+3,2 +3,2	519 520
Sodium-dependent phosphate transport protein 2A	SLC34A1, NaPi-IIa	+2.6	623
Electrogenic sodium bicarbonate cotransporter 1	SLC4A1	+2,4 +3,1 +3,1 +2,6	1029, 1034;985, 990 1069,1071;1025, 1027 1070, 1071;1026,1027 255, 256;211, 212
Sodium/glucose cotransporter 2	SLC5A2	+2.9 +2.9	619 627
Sodium/hydrogen exchanger 3	NHE3	+3.8	588
Neutral and basic amino acid transport protein rBAT	SLC3A1	+3,6 +3,0 +2,8	39 42 49
Y+L amino acid transporter 1	SLC7A7	+2.9	19
Large neutral amino acids transporter small subunit 2	SLC7A8	+2,7 +2,6	28 506
b(0,+)-type amino acid transporter 1	SLC7A9	+3.2	16, 18

Table 4:

Inflammation	Protein Name	Fold change DUSP3-KO/WT	AA-site
Fos-related antigen 2	FRA2	-5,8 -4,0 -4,6 -4,6 -4,8 -4,6 -4,8	120;93 200;173 308, 320;281, 293 308, 322;281, 295 83;56 309, 320;282, 293 82;55
Transcription factor AP-1	c-JUN	-3,1 -3,9 -6,4	246 63 100;73
Nuclear factor NF-kappa-B p100 subunit	NFkB-p100	-3.3	222; 220
Signal transducer and activator of transcription 3	STAT3	-2.9	705
Kidney Injury Molecule-1	KIM-1 (TIM-1)	-21,7 -14,2 -4,1	299;276 279;256 292;269
Lymphocyte-specific protein 1	LSP1	-3,3 -3,3	179, 184;177, 182 180, 184;178, 182
CCAAT/enhancer-binding protein beta	C/EBPβ	-2,6 -2,6 -3,7 -3,7 -3,7	183;162;32 184;163;33 171, 188;150, 167;20, 37 178, 188;157, 167;27, 37 182, 188;161, 167;31, 37
Clusterin	CLU	-5,1	164, 169
Mitogen-activated protein kinase 4	HGK	-2,9 -2,9 -2,6 -2,7 -2,7	556 558 619, 621 794 795
Secreted phosphoprotein 1	SPP1	-12,6 -12,6 -15,3 -23,6 -15,3 -15,6 -15,0 -10,4	219, 228, 231 219, 231, 234 289 289, 291 290 176 247, 250 32

Table 5: Comparative analyses of urines between *wild-type* and *Dusp3*$^{-/-}$ mice at baseline and following renal ischemia/reperfusion

Urine		*WT*		*Dusp3*$^{-/-}$	
	Measurements	***At baseline***	***Post renal I/R***	***At baseline***	***Post renal I/R***
	Urine volume (µl/24 h)	723.60 ± 79.64	639.50 ± 94.33	497.30 ± 73.99	487.10 ± 89.55
	Creatinine (Cr) (mmol/l)	1.91 ± 0,28 *	3.96 ± 0.77 *	2.58 ± 0,22	3.15 ± 0.52
	Uric acid (mmol/mmol Cr)	0.19 ± 0,02 *	0.04 ± 0.01 *	0.24 ± 0.06	0.10 ± 0.02
	Cl^- (mmol/mmol Cr)	85.81 ± 7.66 *	40.19 ± 3.08 *	80.98 ± 8.88 $	41.24 ± 2.96 $
	K^+ (mmol/mmol Cr)	75.63 ± 6,07 *	27.47 ± 3.33 *	66.14 ± 5.50 $	20.67 ± 1.99 $
	Na^+ (mmol/mmol Cr)	74.98 ± 5,01 *	30.40 ± 4.49 *	89.96 ± 7.33 $	28.89 ± 5.27 $
	FeNa (%)	0,24 ± 0,02	0.22 ± 0.04	0,26 ± 0,02	0.24 ± 0.13
	Albumin (mmol/mmol Cr)	0,10 ± 0,01 *	1,42 ± 0,30 * §	0,11 ± 0,01 $	0,68 ± 0,13 $ §
	α1-microglobulin (µmol/mmol Cr)	2.10 ± 0.18 *	4.34 ± 0.45 * §	2.18 ± 0.31	2.90 ± 0.19 §

Table 6: Comparative analyses of plasma between *wild-type* and *Dusp3*$^{-/-}$ mice at baseline and following renal ischemia/reperfusion

Plasma		*WT*		*Dusp3*$^{-/-}$	
	Measurements	***At baseline***	***Post renal I/R***	***At baseline***	***Post renal I/R***
	BUN (mg/dl)	45.19 ± 5.44	138.20 ± 24.27 §	54.16 ± 7.84	52.83 ± 6.77 §
	Cl^- (mmol/l)	106.10 ± 4.82	103.90 ± 2.26	110.0 ± 2.60	94.97 ± 7.30
	K^+ (mmol/l)	4.65 ± 0.14	4,80 ± 1.01	4,29 ± 0,36	3,96 ± 0.09
	Na^+(mmol/l)	175.30 ± 7.99	167,20 ± 3.42	158,60 ± 6,92	162,10 ± 15,81
	SCr (mg/dl)	0.10 ± 0.01	0.60 ± 0.20 §	0.10 ± 0.03	0.13 ± 0.01 §
	GFR (µl/min)	160.70 ± 15,43	76,70 ± 4,78 §	163,70 ± 15,45	164,40 ± 21,31 §

Values are mean ± SEM.

* / $: Paired t-test; §: Unpaired t test ($P < 0.05$).

Figure Legends

Figure 1: (A) Co-localization of DUSP3 with nephrin (marker of podocytes) in *WT* and *Dusp3*$^{-/-}$ mice. DUSP3 is detected in glomerular podocytes (arrows) and endothelial cells (arrow heads). Scale bar = 10 µm. Co-localisation of DUSP3 with meca-23 (marker of fenestrae of endothelial cells) in *WT* and *Dusp3*$^{-/-}$ mice. DUSP3 is most abundantly expressed in nuclei and to lesser extent in the cytoplasm of endothelial cells. Higher magnification inset in the merged image shows DUSP3 in endothelial cells. Scale bar = 50µm. **(B)** Real-time qPCR quantification of mRNA expression level of DUSP3 in *WT sham* (n=9) vs *WT* I/R kidneys (n=10). The Mann-Whitney test was used to assess the statistical significance. Data are presented as mean ± standard deviation. Significant differences are indicated, ‡ p<0,001 versus WT control group. **(C)** Western blot analysis was performed on *WT* sham vs *WT* I/R kidneys to evaluate the expression level of DUSP3. Upon I/R the level of DUSP3 significantly increased (n=6). An unpaired parametric test was used to assess the statistical significance. Data are presented as mean ± standard deviation. Significant differences are indicated, † p<0,01 versus WT control group. **(D)** Immunohistochemistry of DUSP3 co-stained with megalin (marker of proximal tubule) shows strongly augmented DUSP3 expression in proximal tubule cells (asterisk), endothelial cells (arrow head) and podocytes (arrow) following I/R. Scale bar = 50µm.

Figure 2: (A) Levels of serum blood urea nitrogen (BUN) in *WT* (n=10) and *Dusp3*$^{-/-}$ mice (n=10) measured at 48-h post-I/R. An unpaired parametric test was used to assess the statistical significance. **(B)** PAS-stained kidney sections show normal architecture of the tubules in *Dusp3*$^{-/-}$ (n=8) compared to the *WT* (n=9) post I/R. Histologic damage was graded following the Jablonski

score. Individual scores are shown as medians and interquartile range. Chi-square test was used to assess the statistical significance.

Figure 3: (A) Real-time qPCR quantification of mRNA expression levels of *DUSP3, Vascular Endothelial Growth Factor (VEGF)* and *Platelet endothelial cell adhesion molecule (PECAM1 or CD31)* between the two genotypes (n=6). **(B)** Cross-sections of kidneys labeled for vascular density via CD31 in *WT* and *Dusp3*$^{-/-}$ mice. **(C)** *Dusp3*$^{-/-}$ mice (n=12) have a higher renal vascular density compared to *WT* (n=9). **(D)** Representative Color Doppler image for measurement of renal flow velocities. **(E)** Renal resistivity index showed a decreased resistivity in *Dusp3*$^{-/-}$ group (n=9) comparted to *WT* (n=10). Values are presented as individual data points and means. **(F)** Real-time qPCR quantification of mRNA expression levels of *VEGF* on *WT* vs *Dusp3*$^{-/-}$ kidneys post-I/R (n=5). An unpaired parametric test was used to assess the statistical significance. Data are presented as mean ± standard deviation. Significant differences are indicated, * p<0,05; † p<0,01; ‡ p<0,001 versus *WT* control group.

Figure 4: (A) Sequence logo of the group of peptides in the Fe-IMAC analysis that increased quantitatively in abundance with *Dusp3*$^{-/-}$ compared to the full dataset of all peptides identified. Amino acids with positive values are over-represented among peptides that increase with KO while those with negative values are under-represented compared to the full dataset. The sequence analysis highlights, in particular, the preference for Arginine (R) at position -3. Red lines indicate p<0.05 for each position. **(B)** Volcano plot of phosphoproteomic changes plotting p-value *versus* fold-change for all significantly different phosphopeptides between *WT* vs *Dusp3*$^{-/-}$ kidneys post-I/R. Red color: down-regulation. Blue color: Up-regulation. Orange circle: Inflammatory factors; Blue circle: Transport and metabolism factors; Green circle: pro-angiogenic factors. **(C)** Western blot analysis of *P-c-Jun* was performed on *WT* vs *Dusp3*$^{-/-}$ kidneys post-I/R (n=6) with Rab11 as a total protein loading control. Individual samples and the combined samples used for mass spec analysis were analyzed. Signal was normalized based on Rab11 loading to quantify *P-c-Jun* levels. An unpaired parametric test was used to assess the statistical significance.

Figure 5: (A) Real-time qPCR quantification of mRNA expression levels of *Interleukin 6 (IL-6), Intercellular Adhesion Molecule 1 (Icam-1 or CD11b), Interleukin 1b (IL-1b), Kidney Injury Molecule 1 (Kim- 1), Caspase-3 (Caspase) and Tumor necrosis factor (TNF)* in the kidney after 30

minutes of ischemia followed by 48 hours of reperfusion (I/R). All values of *WT* I/R and *Dusp3*$^{-/-}$ I/R were normalized to *WT* sham expression. **(B)** Representative Immunoblotting and quantification of Intercellular Adhesion Molecule 1 (Icam-1 or CD11b), Heat Shock Protein 70 (HSP70) and Proliferating cell nuclear antigen (PCNA) in *WT* I/R and *Dusp3*$^{-/-}$ I/R kidneys. A Mann-Whitney test was used to assess the statistical significance. **(C)** Immunohistochemistry on I/R kidneys of *WT* and *DUSP3*$^{-/-}$ mice for cell proliferation (PCNA), infiltration of inflammatory cells (CD11b) and total macrophage population (F4/80). Quantification of positive cells (arrow heads) in the cortico-medullary section of kidney, unpaired parametric T-test was used to assess the statistical significance. Data are presented as mean ± standard deviation. Significant differences are indicated, * $p<0,05$; † $p<0,01$; ‡ $p<0,001$ versus *WT* control group.

Figure 1: DUSP3 is expressed in the renal parenchyma

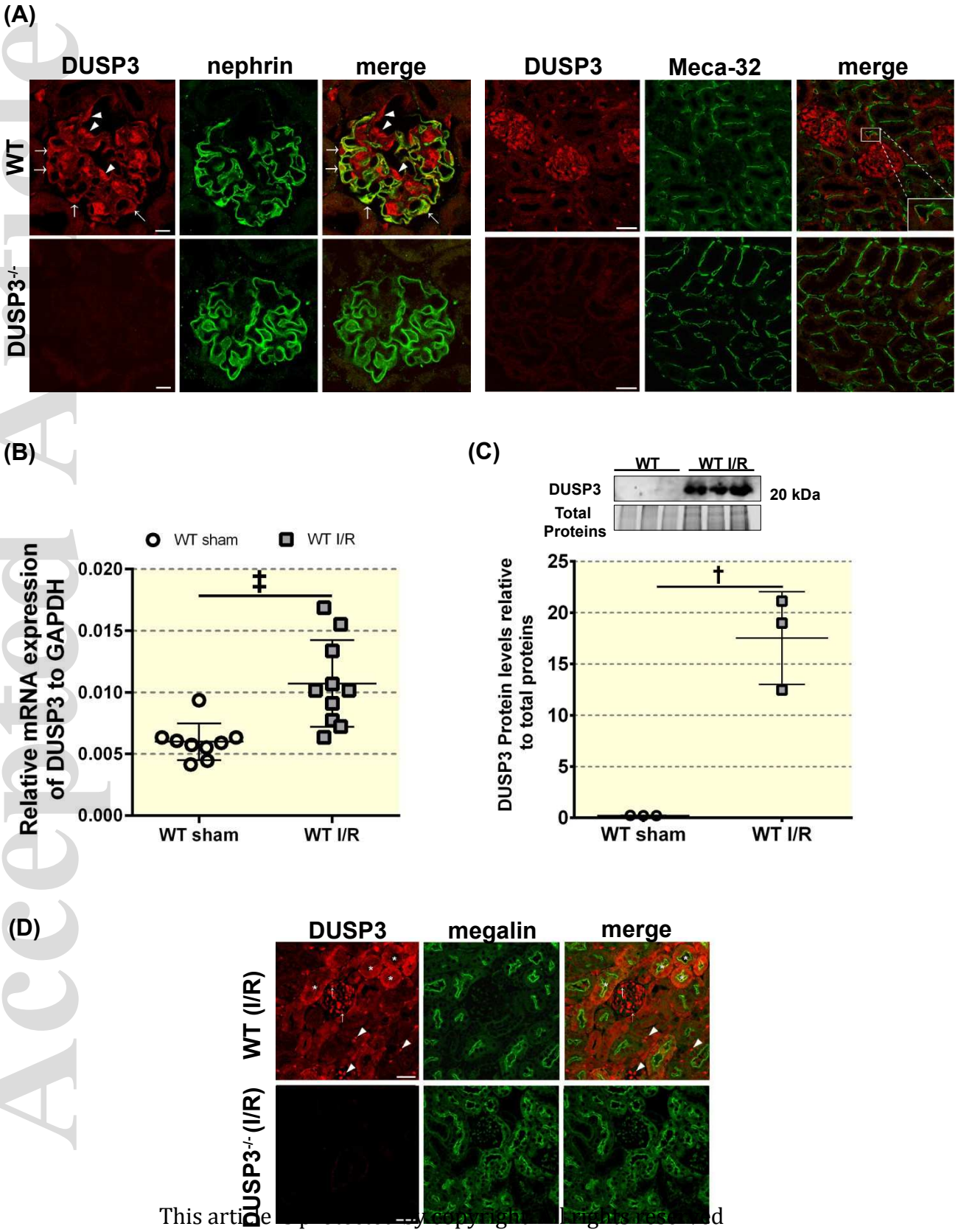

* p<0,05; † p<0,01; ‡ p<0,001

Figure 2: *Dusp3*$^{-/-}$ mice are resistant to renal I/R injury

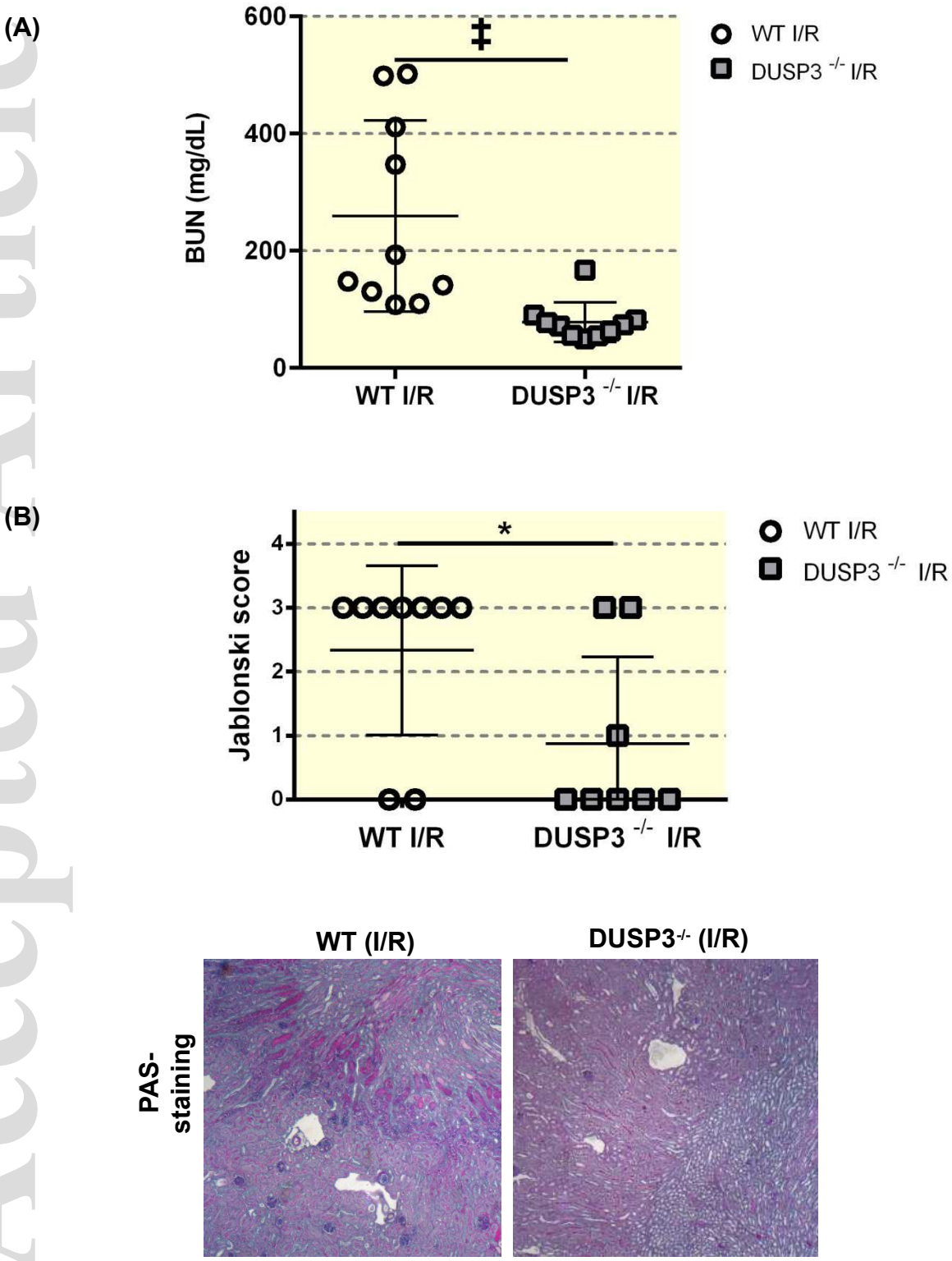

* p<0,05; † p<0,01; ‡ p<0,001

Figure 3: *Dusp3*$^{-/-}$ kidneys show an increased renal vascular density

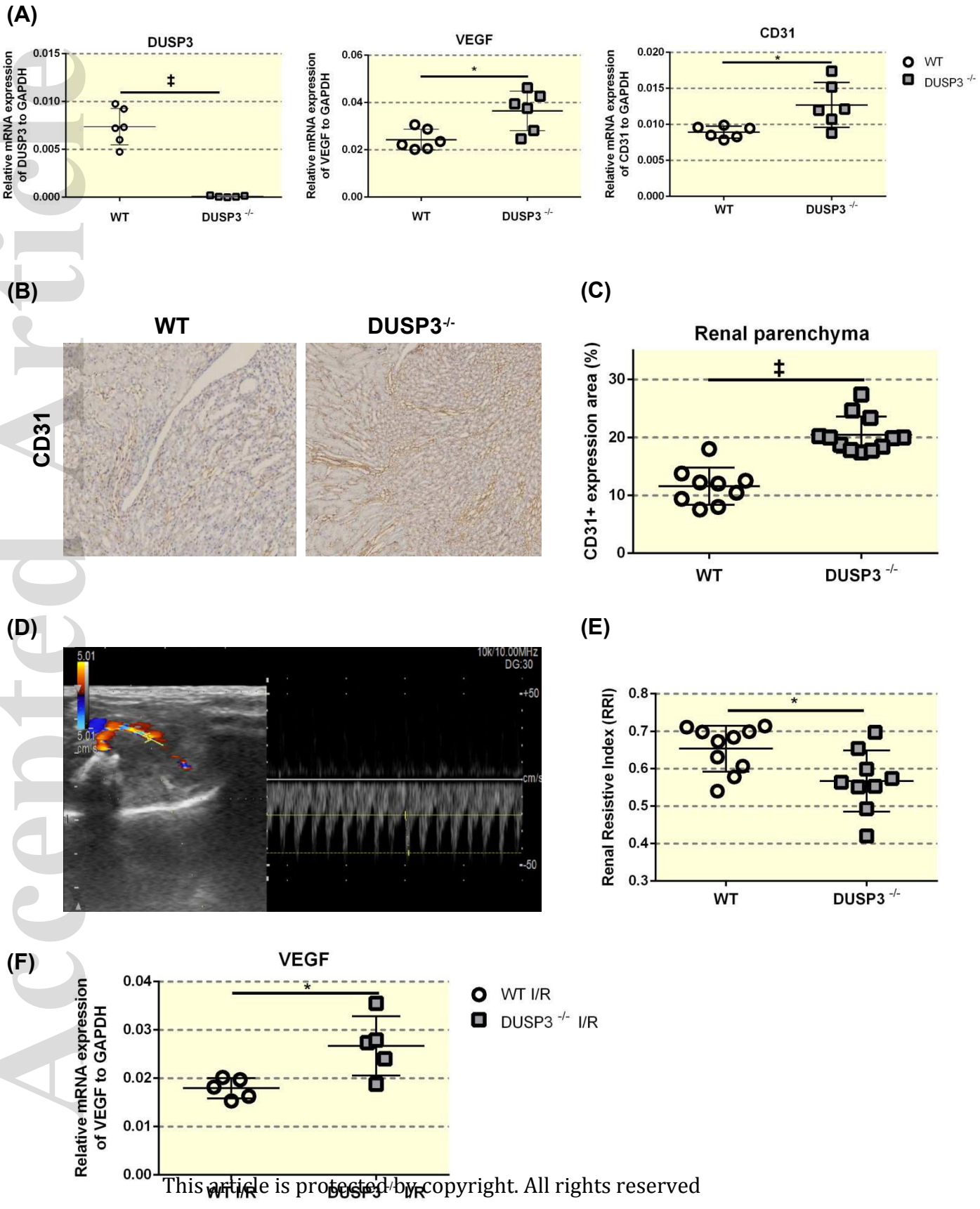

* p<0,05; † p<0,01; ‡ p<0,001

Figure 4: Comparative phosphoproteomics between *Dusp3*$^{-/-}$ and *WT* kidneys *post*-I/R

(A)

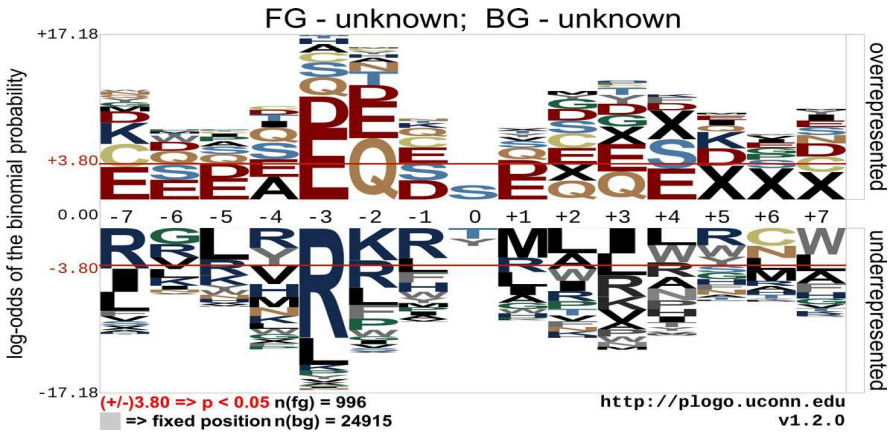

(B)

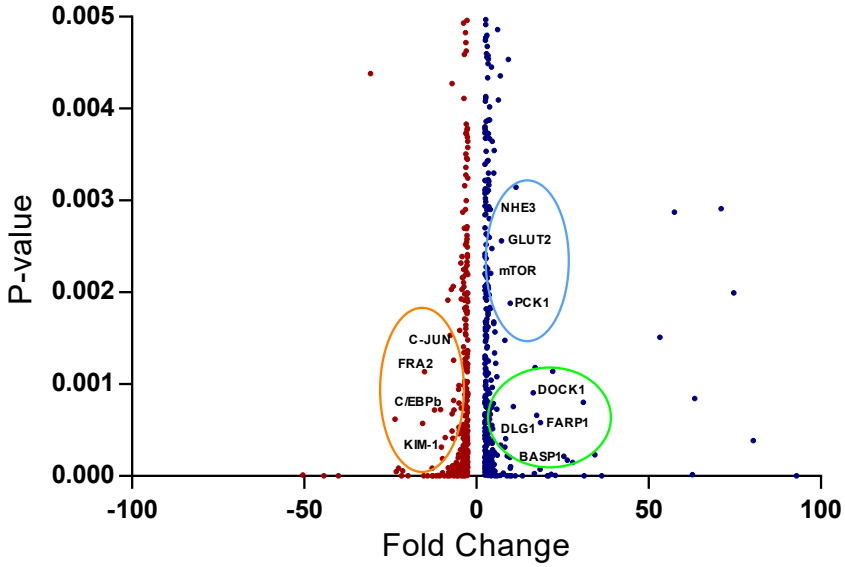

(C)

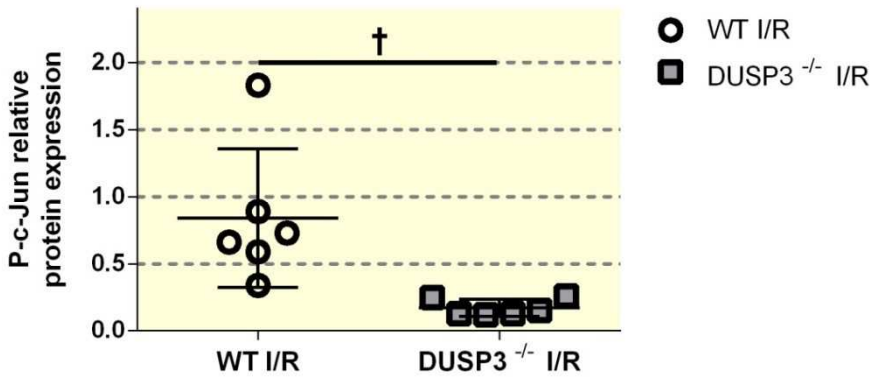

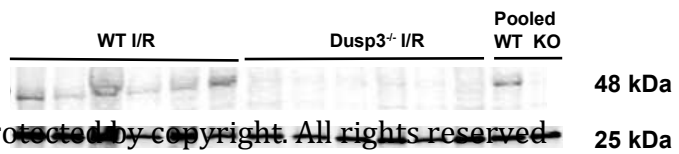

* p<0,05; † p<0,01; ‡ p<0,001

Figure 5: *Dusp3*$^{-/-}$ kidneys exposed to I/R show an attenuated inflammatory response

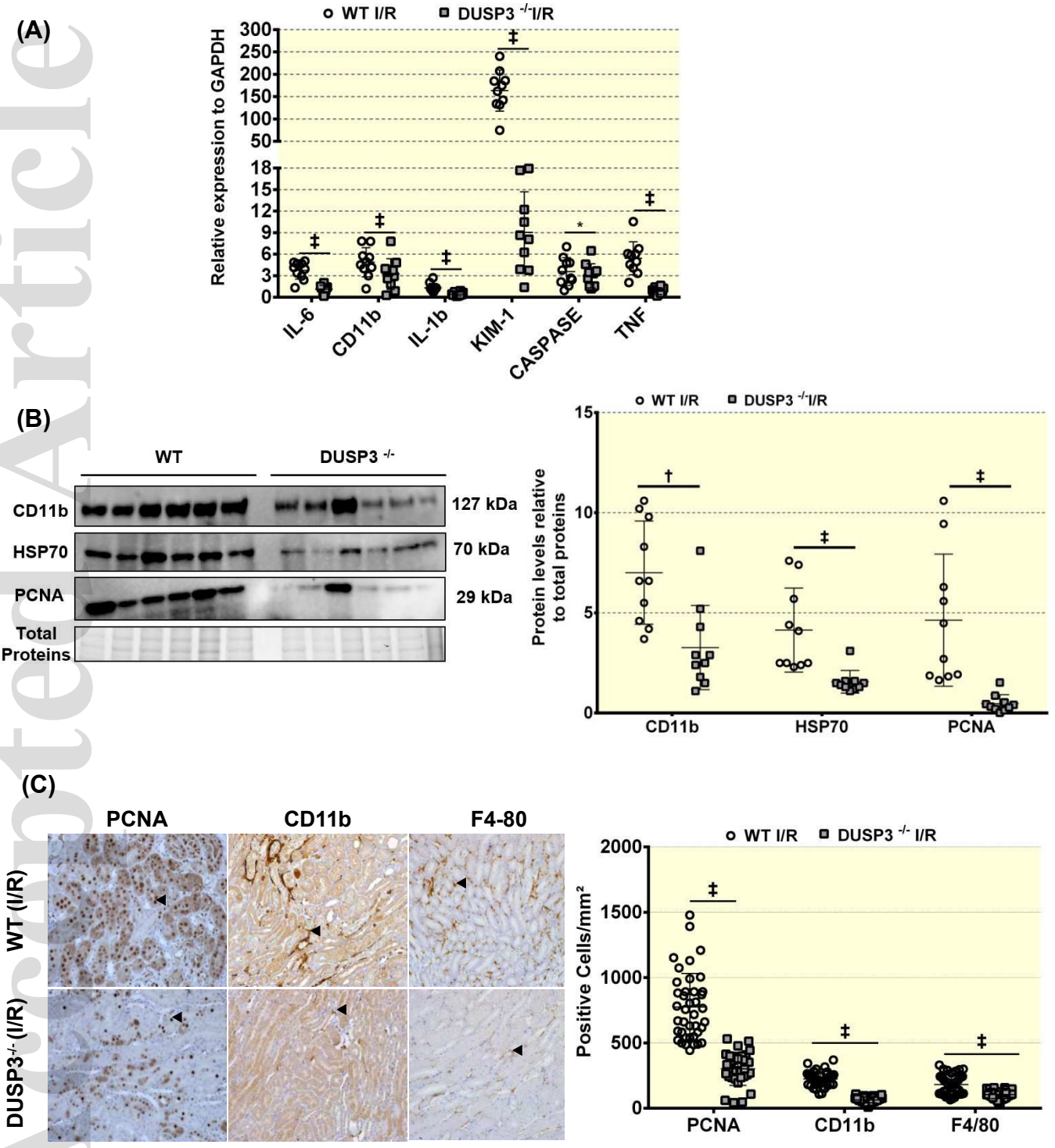

* p<0,05; † p<0,01; ‡ p<0,001